

# Time-dependent electron localisation function: A tool to visualise and analyse ultrafast processes

Alberto Castro,<sup>1</sup> Tobias Burnus,<sup>2</sup> M. A. L. Marques,<sup>3</sup> and E. K. U. Gross<sup>4</sup>

<sup>1</sup>*Institut für Theoretische Physik, Fachbereich Physik der Freie Universität Berlin, Arnimallee 14, D-14195 Berlin (Germany)*

<sup>2</sup>*Physikalisches Institut, Universität zu Köln, Zùlpicher Str. 77, D-50937 Köln (Germany)*

<sup>3</sup>*Departamento de Física, Universidade de Coimbra, Rua Larga, 3004-516 Coimbra (Portugal)*

<sup>4</sup>*Institut für Theoretische Physik, Fachbereich Physik der Freie Universität Berlin, Arnimallee 14, 14195 Berlin (Germany)*

in *Analysis and Control of Ultrafast Photoinduced Reactions*,

O. Kün and L. Wöste (Eds.), Springer Series in Chemical Physics **87**, Springer, Heidelberg (2007), Chapter 6.5.

The classical picture of chemical bonding in terms of electron pairs that are shared by atoms in order to form molecules was nicely systematized by G. N. Lewis, in his seminal work entitled “The Atom and the Molecule”<sup>1</sup>, dated 1916. Lewis noticed the overwhelming evidence pointing to the “pairing” of the electrons, as well as the preference to close “shells” of eight electrons. Soon afterwards, the pairing of electrons was explained in terms of the Pauli exclusion principle together with the electronic intrinsic one-half spin, whereas the number eight in fact emanates from both Pauli’s principle and the spherical symmetry of atoms in a three dimensional world. Lewis, however, was some years too early, and designed “the theory of the cubical atom”, with the electrons occupying the vertex of a cube (although he acknowledged the picture to be more methodological than fact-founded), and pointed to a breakdown of Coulomb law at short distances in order to explain the electron pairs. Despite these exotic suggestions, the usefulness of Lewis model has persisted even until today’s textbooks.

The reason is that electrons do indeed “localize” in pairs when forming molecules, and a big amount of the basic machinery of Chemistry is rather well explained with Lewis arguments. In fact, more generally, Chemistry is intuitively understood in terms of “localized” groups of electrons, either pairs of electrons shared between atoms (“bonds”), non-bonding pairs of electrons (“lone pairs”), and also larger groups – double, triple bonds –, atomic inner shells,  $\pi$  electronic systems, etc.

With the advent, in the past years, of sources of coherent light featuring high intensity and ultrafast pulses (in the femtosecond<sup>2</sup>, or already below the femtosecond limit<sup>3</sup>), it has become possible to *time resolve* the intermediate steps of chemical reactions – paving the way to the possibility of analyzing and controlling chemical reactions. These technical advances stress the need of understanding how the electrons rearrange, forming and destroying bonds, in the midst of a laser pulse, and during the possible ionic recombination. The chemical concepts of bonds, lone pairs, etc, have to be fathomed also for time-dependent phenomena.

Unfortunately, the transformation of these concepts into a mathematically rigorous scheme for classifying the elements of the chemical bonding turns out to be astonishingly difficult. The canonical single-particle orbitals that stem from Hartree-Fock (HF) calculations are not very helpful, since they, typically, have sizable contributions from many regions in space. Moreover, they are only one possible choice, since unitary transformations within the subspace of solutions yield equally legitimate orbitals. There are several ways in which one can perform these unitary transformations in order to obtain localized functions<sup>4</sup>, but these methods are also not unique, and may result in qualitatively different information.

In any case, HF is but one of the possible schemes to obtain an approximate solution to the many-body problem. A definition based on the HF solution would always be affected by the HF error – absence of correlation effects. It is desirable to have a scheme that does not rely on a particular method. Kohn-Sham (KS)<sup>5</sup> density functional theory (DFT)<sup>6–8</sup> also provides single-particle orbitals (in this case unique, except for degenerate ground-states), but they are usually also very delocalized in real-space. The electronic density is an observable, and thus independent of the method. Moreover, it contains all the information of the system by virtue of Hohenberg-Kohn theorem<sup>9</sup>. Unfortunately, the density itself is not suitable to visualize chemical bonding: It does not peak in the position of the bonds, it does not show the shell structure of atoms, and lone pairs, also, are poorly represented.

The key to comprehending electron localization is, in fact, Pauli’s exclusion principle, and, relatedly, the Fermi hole: Bader and collaborators<sup>10</sup> demonstrated how all manifestations of the spatial localization of an electron of a given spin are the result of corresponding localizations of its Fermi hole. An appropriate localization function should be closely related to this Fermi hole or to an analysis of Pauli’s principle. This is indeed the case for the function to which we devote this section: Becke and Edgecombe’s electron localization function<sup>11</sup> (ELF), as generalized by Burnus, Marques and Gross for time-dependent cases<sup>12</sup>. The next subsection will show how the Fermi hole appears naturally in the derivation of the ELF.

An alternative way to rationalize the ELF definition is to think in terms of how Pauli’s exclusion principle affects

the kinetic energy. This principle applies to fermionic systems; the kinetic energy of a bosonic system is a lower bound to the local kinetic energy of a fermionic one<sup>13</sup>. Thus we can define an *excess kinetic energy*, which would be the difference between the two of them. Intuitively, in a region of electron localization (electrons forming pairs, isolated electrons), their behavior is more bosonic-like. So we will require, to define localization, that the excess kinetic energy is minimized. This is indeed the case for the ELF, as it will be demonstrated later.

The ELF, as introduced by Becke and Edgecombe, involved two approximations: (i) First, it assumed that the many-electron wave function is a single Slater determinant. The natural choice is the Hartree-Fock solution. (ii) Second, it assumed that the single-particle orbitals that form the single Slater determinant, are *real functions*. This prevents its validity in a time-dependent formalism, or for static but current-carrying states. A generalized derivation that lifted this restriction was presented by Dobson<sup>14</sup>, and later by Burnus, Marques and Gross<sup>12</sup> who demonstrated how this general form could be applied for time-dependent processes. The observation of this function is useful for the study of chemical reactions and for processes that involve the interaction of molecular systems with high-intensity ultra-short laser pulses (femtosecond or even attosecond regime), or collision processes between molecules and/or ions. In this time scale, and for these probably violent deformations of the molecular fields, the electrons are bound to exhibit a complex behavior: bonds are destroyed or created, bond types change as the molecules isomerize, dissociate, or recombine in chemical reactions. These events are especially patent in the evolution of the ELF.

Next subsection is dedicated to the definition of the (possibly time-dependent) ELF. In Sect. B, some examples of the ELF for systems in the ground state are shown, in order to illustrate the association between ELF topological features and Chemistry bonding elements. Sect. C provides examples of time-dependent calculations in which the TDEL is monitored: collision processes leading to chemical reactions, and interaction of molecules with laser pulses. The chapter closes, in Sect. D, with an example in which the coupled evolution of electrons and nuclei, both treated quantum-mechanical, is computed for a model system. The ELF is then used to learn about the strength of non-adiabatic effects.

## A. The time-dependent electron localization function

### 1. General definition

We depart from the definitions of the one and two-body density matrices for a system of  $N$  electrons<sup>15,16</sup>, whose evolution is described by the wave function  $\Psi(\mathbf{r}_1\sigma_1, \dots, \mathbf{r}_N\sigma_N; t)$ :

$$\Gamma_{\sigma_1|\sigma'_1}^{(1)}(\mathbf{r}_1|\mathbf{r}'_1; t) = N \sum_{\sigma_2, \dots, \sigma_N} \int d^3r_2 \dots \int d^3r_N \Psi^*(\mathbf{r}_1\sigma_1, \mathbf{r}_2\sigma_2, \dots, \mathbf{r}_N\sigma_N; t) \times \Psi(\mathbf{r}'_1\sigma'_1, \mathbf{r}_2\sigma_2, \dots, \mathbf{r}_N\sigma_N; t), \quad (1)$$

$$\Gamma_{\sigma_1\sigma_2|\sigma'_1\sigma'_2}^{(2)}(\mathbf{r}_1, \mathbf{r}_2|\mathbf{r}'_1\mathbf{r}'_2; t) = N(N-1) \sum_{\sigma_3, \dots, \sigma_N} \int d^3r_3 \dots \int d^3r_N \Psi^*(\mathbf{r}_1\sigma_1, \mathbf{r}_2\sigma_2, \dots, \mathbf{r}_N\sigma_N; t) \Psi(\mathbf{r}'_1\sigma'_1, \mathbf{r}'_2\sigma'_2, \dots, \mathbf{r}_N\sigma_N; t). \quad (2)$$

The spin-densities are defined in terms of the diagonal one-body density matrix:

$$n_\sigma(\mathbf{r}, t) = \Gamma_{\sigma|\sigma}^{(1)}(\mathbf{r}|\mathbf{r}; t). \quad (3)$$

For equal spin ( $\sigma_1 = \sigma_2 = \sigma$ ), the diagonal of the two-body density matrix,  $\Gamma_{\sigma\sigma|\sigma\sigma}^{(2)}(\mathbf{r}_1, \mathbf{r}_2|\mathbf{r}_1\mathbf{r}_2; t)$ , is the same-spin pair probability function,  $D_\sigma(\mathbf{r}_1, \mathbf{r}_2; t)$ . Its value is the probability of finding one electron at  $\mathbf{r}_1$  and another electron at  $\mathbf{r}_2$ , both with the same spin  $\sigma$ :

$$D_\sigma(\mathbf{r}_1, \mathbf{r}_2; t) = \Gamma_{\sigma\sigma|\sigma\sigma}^{(2)}(\mathbf{r}_1, \mathbf{r}_2|\mathbf{r}_1, \mathbf{r}_2; t). \quad (4)$$

If the electrons were *uncorrelated*, the probability of finding the pair of electrons at  $\mathbf{r}_1$  and  $\mathbf{r}_2$  would be the product of the individual probabilities:  $D_\sigma(\mathbf{r}_1, \mathbf{r}_2; t) = n_\sigma(\mathbf{r}_1; t)n_\sigma(\mathbf{r}_2; t)$ . Electrons are, however, correlated, and the same-spin pair density is less than that value by a factor that is defined as the *pair correlation function*:

$$D_\sigma(\mathbf{r}_1, \mathbf{r}_2; t) = n_\sigma(\mathbf{r}_1; t)n_\sigma(\mathbf{r}_2; t)g_{\sigma\sigma}(\mathbf{r}_1, \mathbf{r}_2; t). \quad (5)$$

The difference between the correlated and the uncorrelated case is also contained in the *Fermi hole* function  $h_\sigma(\mathbf{r}_1, \mathbf{r}_2; t)$ :

$$D_\sigma(\mathbf{r}_1, \mathbf{r}_2; t) = n_\sigma(\mathbf{r}_1; t) (n_\sigma(\mathbf{r}_2; t) + h_{\sigma\sigma}(\mathbf{r}_1, \mathbf{r}_2; t)). \quad (6)$$

The same-spin *conditional* probability function,  $P_\sigma(\mathbf{r}_1, \mathbf{r}_2; t)$  is then defined as the probability of finding a  $\sigma$ -spin electron at  $\mathbf{r}_2$ , knowing that there is one  $\sigma$ -spin electron at  $\mathbf{r}_1$ . It can be expressed in terms of the previous definitions:

$$\begin{aligned} P_\sigma(\mathbf{r}_1, \mathbf{r}_2; t) &= \frac{D_\sigma(\mathbf{r}_1, \mathbf{r}_2; t)}{n_\sigma(\mathbf{r}_1; t)} = n_\sigma(\mathbf{r}_2; t) g_{\sigma\sigma'}(\mathbf{r}_1, \mathbf{r}_2; t) \\ &= n_\sigma(\mathbf{r}_2; t) + h_{\sigma\sigma}(\mathbf{r}_1, \mathbf{r}_2; t). \end{aligned} \quad (7)$$

From this equation, the meaning of the Fermi hole (a negative function at all points) is more transparent: it is a measure of how probability at  $\mathbf{r}_2$  is reduced due to the spreading out of the same spin density originated at  $\mathbf{r}_1$ .

However, it will be more useful to define an alternative same-spin conditional pair probability function: given a reference electron of  $\sigma$ -spin at  $\mathbf{r}$ , we are interested in the probability of finding a same-spin electron at a distance  $s$ . This involves taking a spherical average on a sphere of radius  $s$  around point  $\mathbf{r}$ ,  $S(s, \mathbf{r})$ :

$$p_\sigma(\mathbf{r}, s; t) = \frac{1}{4\pi} \int_{S(s, \mathbf{r})} dS P_\sigma(\mathbf{r}, \mathbf{r}'; t). \quad (8)$$

The integration is done for the  $\mathbf{r}'$  variable. For small values of  $s$  one can obtain the following Taylor expansion:

$$p_\sigma(\mathbf{r}, s; t) = \frac{1}{3} \left[ \frac{1}{2} \frac{[\nabla_{\mathbf{r}'}^2 D_\sigma(\mathbf{r}, \mathbf{r}'; t)]_{\mathbf{r}'=\mathbf{r}}}{n_\sigma(\mathbf{r}, t)} \right] s^2 + \mathcal{O}(s^3). \quad (9)$$

In this expansion, the term in  $s^0$  is absent due to the Pauli exclusion principle. The linear term in  $s$  is also null<sup>17</sup>. The coefficient of  $s^2$  (except for the one-third factor) thus tells us about the same-spin pair probability in the vicinity of  $\mathbf{r}$ :

$$C_\sigma(\mathbf{r}) = \frac{1}{2} \frac{[\nabla_{\mathbf{r}'}^2 D_\sigma(\mathbf{r}, \mathbf{r}'; t)]_{\mathbf{r}'=\mathbf{r}}}{n_\sigma(\mathbf{r}, t)}. \quad (10)$$

This function is an *inverse* measure of localization: it tells us how large the same-spin conditional probability function is at each point in space. The smaller this magnitude is, the more likely than an electron *avoids* electrons of equal spin.

In addition to having an inverse relationship to localization – for example, it is null for perfect localization –,  $C_\sigma$  is not bounded by above. Visually, it does not mark the chemical structure with great contrast. These reasons led to Becke and Edgecombe to suggest a re-scaling, noticing that, for the homogeneous electron gas,  $C_\sigma$  is nothing else than the kinetic energy density (atomic units will be used in all equations of this section):

$$C_\sigma^{\text{HEG}} = \tau_\sigma^{\text{HEG}} = \frac{3}{5} (6\pi^2)^{(2/3)} n_\sigma^{(5/3)}. \quad (11)$$

One may then refer the value of  $C_\sigma$  at each point to the value that the homogeneous electron gas would have for the density of that point at that time  $t$ ,  $C_\sigma^{\text{HEG}}(\mathbf{r}; t)$ . Moreover, since there is an inverse relationship between  $C_\sigma$  and localization, it is useful to invert it. The final expression for the “electron localization function”,  $\eta_\sigma(\mathbf{r})$ , is

$$\eta_\sigma(\mathbf{r}; t) = \frac{1}{1 + (C_\sigma(\mathbf{r}; t)/C_\sigma^{\text{HEG}}(\mathbf{r}; t))^2}. \quad (12)$$

## 2. Expression for one-determinantal wave functions

Up to this point, the equations allow for complete generality. Equation (12) in particular, together with (10), defines the ELF for any system, either in the ground state or in a time-dependent situation, and regardless of which scheme is chosen to approximate a solution to the many electron problem. However, the ELF was originally introduced assuming a Hartree-Fock formulation (one determinantal character of the many-body wave function). The formulation may thus be translated to the Kohn-Sham (KS) formulation of density-functional theory (DFT).

For one-determinantal wave functions, the function  $C_\sigma$  (10) may be explicitly calculated. Let us assume the Slater determinant to be formed of the orbitals  $\{\varphi_{i\uparrow}\}_{i=1}^{N_\uparrow}$  and  $\{\varphi_{i\downarrow}\}_{i=1}^{N_\downarrow}$ , for spin up and down, respectively ( $N = N_\uparrow + N_\downarrow$ ). In this case, one can use the two following identities:

$$\Gamma^{(1)}(\mathbf{r}_1\sigma|\mathbf{r}_2\sigma;t) = \sum_{i=1}^{N_\sigma} \varphi_{i\sigma}^*(\mathbf{r}_2;t)\varphi_{i\sigma}(\mathbf{r}_1;t). \quad (13)$$

$$\text{(This implies immediately: } n_\sigma(\mathbf{r},t) = \sum_{i=1}^{N_\sigma} |\varphi_{i\sigma}(\mathbf{r},t)|^2 \text{.)}$$

$$D_\sigma(\mathbf{r}_1,\mathbf{r}_2;t) = n_\sigma(\mathbf{r}_1;t)n_\sigma(\mathbf{r}_2;t) - |\Gamma^{(1)}(\mathbf{r}_1\sigma|\mathbf{r}_2\sigma;t)|^2. \quad (14)$$

Equations (13) and (14) are then introduced in the expression for  $C_\sigma$ , (10):

$$C_\sigma(\mathbf{r};t) = \frac{1}{2} [\nabla_{\mathbf{r}'}^2 n_\sigma(\mathbf{r}';t)]_{\mathbf{r}'=\mathbf{r}} - \frac{1}{2} \left[ \nabla_{\mathbf{r}'}^2 \frac{|\Gamma^{(1)}(\mathbf{r}'|\mathbf{r};t)|^2}{n_\sigma(\mathbf{r};t)} \right]_{\mathbf{r}'=\mathbf{r}}. \quad (15)$$

And after some algebra<sup>18</sup>:

$$C_\sigma(\mathbf{r};t) = \tau_\sigma(\mathbf{r};t) - \frac{1}{4} \frac{(\nabla n_\sigma(\mathbf{r};t))^2}{n_\sigma(\mathbf{r};t)} - \frac{j_\sigma^2(\mathbf{r};t)}{n_\sigma(\mathbf{r};t)}. \quad (16)$$

where  $\tau_\sigma(\mathbf{r};t)$  is the kinetic energy density,

$$\tau_\sigma(\mathbf{r};t) = \sum_{i=1}^{N_\sigma} |\nabla \varphi_{i\sigma}(\mathbf{r};t)|^2, \quad (17)$$

and  $j_\sigma^2(\mathbf{r};t)$  is the squared modulus of the current density:

$$\begin{aligned} \mathbf{j}_\sigma(\mathbf{r};t) &= \langle \Psi(t) | \frac{1}{2m} \sum_{i=1}^N [\delta(\mathbf{r} - \hat{\mathbf{r}}_i) \delta_{\sigma\sigma_i} \hat{\mathbf{p}}_i + \hat{\mathbf{p}}_i \delta(\mathbf{r} - \hat{\mathbf{r}}_i) \delta_{\sigma\sigma_i}] | \Psi(t) \rangle = \\ &= \frac{1}{2i} \sum_{i=1}^{N_\sigma} [\varphi_{i\sigma}^*(\mathbf{r};t) \nabla \varphi_{i\sigma}(\mathbf{r};t) - \varphi_{i\sigma}(\mathbf{r};t) \nabla \varphi_{i\sigma}^*(\mathbf{r};t)]. \end{aligned} \quad (18)$$

Expression (16), upon substitution in (12), leads to the general form for the ELF, if one assumes one-determinantal wave functions. In the original derivation, however, a further restriction was introduced from the beginning: the system is assumed to be in the a stationary state, and the single-particle orbitals are real, which implies zero current. The derivation presented above<sup>12,18</sup>, however, allows for time-dependent Slater determinants (and complex ground-states with non-null current).

The original, “static” ELF, is simply obtained by eliminating the current term from the expression for  $C_\sigma$  (16):

$$C_\sigma^{\text{static}}(\mathbf{r}) = \tau_\sigma(\mathbf{r}) - \frac{1}{4} \frac{(\nabla n_\sigma(\mathbf{r}))^2}{n_\sigma(\mathbf{r})}, \quad (19)$$

and plugging this formula in the ELF definition, (12).

At this point, it is worth noting that this expression is nothing else than the “excess kinetic energy” mentioned in the introduction of this Section. The first term,  $\tau(\mathbf{r})$  (summing over the two spins) is the local kinetic energy of the electronic system. A bosonic system of equal density  $n$ , at its ground state, will concentrate all particles at the ground state orbital,  $\sqrt{n}/N$ . From this fact it follows that the second term of the previous equation is the kinetic energy density of the bosonic system. It is thus clear how the high localization corresponds to a minimization of the excess kinetic energy.

### 3. Density-functional theory approximation to the ELF

It is useful to briefly recall here the essential equations of DFT<sup>6–8</sup> and of TDDFT<sup>19–24</sup>, since these are the theories that are employed to obtain the orbitals from which the ELF is calculated in the examples presented in the following subsection.

There exists a one-to-one correspondence between the ground-state density of a many electron system,  $n$ , and its external potential  $v$ . This permits to write every observable as a functional of the density. For each interacting system, there also exists an auxiliary non-interacting system of fermions, subject to an external potential different to the one in the original system, such that the densities of the two systems are identical. One can then solve this non-interacting system, and obtain any observable of the interacting system by using the appropriate functional of the density.

The one-particle equations that provide the single-particle orbitals that conform the one-determinantal solution to the non-interacting problem are the so-called Kohn-Sham equations:

$$\left\{-\frac{1}{2}\nabla^2 + v_{\text{KS}}(\mathbf{r})\right\} \varphi_i(\mathbf{r}) = \varepsilon_i \varphi_i(\mathbf{r}), \quad i = 1, \dots, N. \quad (20)$$

The density of both the interacting and non-interacting system is then simply:

$$n(\mathbf{r}) = \sum_{i=1}^N |\varphi_i(\mathbf{r})|^2. \quad (21)$$

The problem lies in the calculation of the Kohn-Sham potential,  $v_{\text{KS}}(\mathbf{r})$ , itself a functional of the density. For this purpose, it is usually split into a known and an unknown part – the latter being the so-called exchange and correlation potential  $v_{\text{xc}}(\mathbf{r})$ :

$$v_{\text{KS}}(\mathbf{r}) = v(\mathbf{r}) + \int d^3r' \frac{n(\mathbf{r}')}{|\mathbf{r} - \mathbf{r}'|} + v_{\text{xc}}(\mathbf{r}). \quad (22)$$

TDDFT extends the parallelism between the interacting and the non-interacting system to time-dependent systems<sup>19</sup>. One then has to deal with time-dependent Kohn-Sham equations:

$$i \frac{\partial \varphi_i}{\partial t}(\mathbf{r}; t) = \left\{-\frac{1}{2}\nabla^2 + v_{\text{KS}}(\mathbf{r}; t)\right\} \varphi_i(\mathbf{r}; t), \quad i = 1, \dots, N. \quad (23)$$

Once again, an approximation to a time-dependent exchange and correlation potential is needed.

The ELF is calculated in terms of spin-orbitals, and is not an explicit functional of the density. One may then approximate the ELF of the interacting system by considering the ELF of its corresponding Kohn-Sham system – whose state is a Slater determinant, and can be calculated using the previous equations. Note that this is a completely different approximation to the one taken by considering the Hartree-Fock ELF – even if it leads to an analogous expression. However, it has been shown that the main features of the ELF are rather insensitive to the method utilized in its calculation<sup>25,26</sup>, even for more approximate schemes such as the extended Hückel model.

### B. Examples in the ground-state

This subsection will present some applications of the ELF for systems in the ground state. All calculations have been done within the KS/DFT formalism. For the exchange-correlation potential, the local-density approximation (LDA) has been employed in all cases, except for the water molecule and the hydroxide ion, for which – both in the ground state calculations and in the collision processes presented in the next subsection – the self-interaction correction was added. The resulting functional is orbital dependent, and in order to calculate it, one has to make use of the optimized effective potential theory – together, in this case, with the approximation of Krieger, Li and Iafrate<sup>27</sup>. The functions are represented on a real-space regular rectangular grid (base-less approach). The pseudo-potential approach is taken for the ion-electron interaction, and in order to avoid the explicit treatment of the chemically inert core electrons.<sup>39</sup> The motion of the cores is treated classically. The computations have been carried out with the octopus code<sup>28,29</sup>.

In order to appreciate the usefulness of the ELF to monitor fast, time-dependent molecular processes, it is important to learn the characteristics of the ELF in the ground state. Silvi and Savin<sup>30</sup> outlined a proposal for the classification of chemical bonds based on the topological analysis of the ELF. Let us recall here some basic ideas, illustrated below

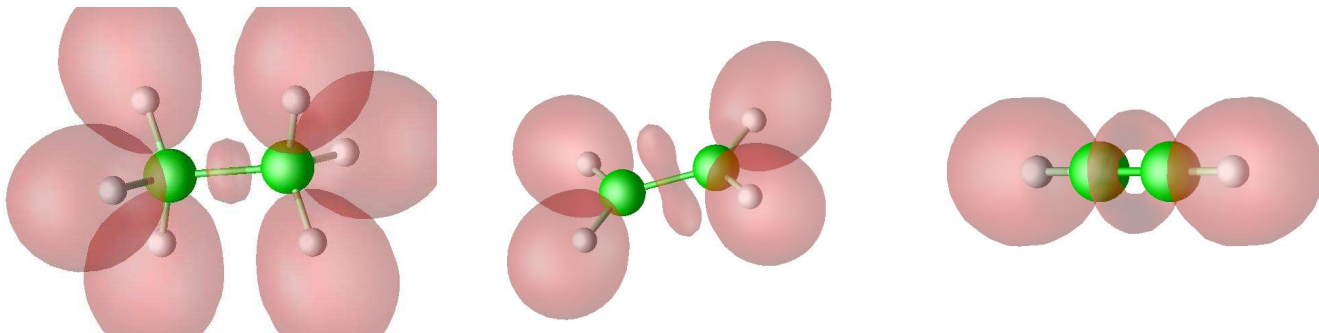


FIG. 1: ELF isosurfaces ( $\eta = 0.85$ ) of ethane (left), ethene (centre) and ethyne (right).

with some examples. The ELF is a scalar real function, bounded between zero and one – the value one corresponding to maximum localization. The *attractors* are the points where it has maxima; to each attractor corresponds a *basin*, the set of points whose gradient field drives to the attractor. The shape of the isosurfaces of the ELF is also informative: as we change the isosurface value, it may or may not change – when it does, we have a *bifurcation*, which occurs at ELF *critical values*. The attractors may have zero, one, or two dimensions: In general, only zero dimensional attractor are allowed; however system with spherical symmetry (atoms) will have spherical (2D) attractor manifolds, whereas  $C_{\infty v}$  (or higher) systems (linear molecules) may have one-dimensional sets of attractors, forming a ring around the molecular axis.

To each attractor one may associate an *irreducible f-localization domain*. An *f-localization domain* is the set of connected points for which the ELF is larger than  $f$ . It is irreducible if it only contains one attractor. The spatial arrangement of these domains is the key to classify chemical bonds: there are three types of attractors: core (its domain contains a nuclei), bonding (located between the core attractors of different atoms) and non-bonding (the rest, that contain the so-called lone pairs). All atoms will have an associated core attractor, except Hydrogen.

In each domain, one may integrate the electronic density, and obtain a number of electrons. In the absence of symmetry, at most two electrons with opposite spins should be found in a basin. An attractor for which the number of electrons in its associated domain is less than two is an *unsaturated attractor*. A multiple bond is created when there is more than one bonding attractor between two core attractors. A ring attractor containing six electrons is also a multiple bond.

A first illustrative example is the clear distinction between the single, double and triple bonds of the ethane, ethene and ethyne molecules, as presented in Fig. 1. The ethyne (acetylene) molecule is an example of linear molecule ( $D_{\infty h}$  symmetry), which allows for continuous ring attractors. These may occur specially for cases in which one expects a triple bond, such as is the case in acetylene. However, other textbook “Lewis” triple bonds do not show a ring attractor: the Nitrogen molecule presents only one point attractor between the nuclei, and two other point attractor at their sides. The double bond of ethene (center in Fig. 1) is clearly manifested by the presence of two attractors between the Carbons. This leads to isosurfaces with a characteristic “eight” shape. The ethane molecule (left), presents only one attractor between the Carbons (single bond), and the six domains corresponding to the CH bonds.

It is known that the ring isomer of  $\text{C}_{20}$  (see Fig. 2, left side) does not have a 20th order axis of symmetry, due to the presence of alternating bonds, which reduces the molecule symmetry group to  $C_{10h}$ . The different nature of the bonds (“single-triple alternation”, in the Lewis picture), is clearly patent in the ELF: the continuous ring of attractors for the triple bonds, whereas one single point attractor for the single bonds. In the case of the  $\text{C}_{60}$  fullerene (see Fig. 2, right side) due to its high symmetry, there are also in principle two possibly different kinds of bonds: the ones for which the bond line is separating two hexagons, and the ones for which the bond line is separating one pentagon and one hexagon. A look at the ELF tells us that the character of these bonds is, however, very similar.

The usefulness of the ELF is specially patent for the analysis of non-bonding electron groups<sup>31</sup>. In Fig. 3 two examples are shown: the hydroxide ( $\text{OH}^-$ ) ion, and the water molecule. In the first case (right), there is once again a continuous ring attractor, that contains six electrons. This reflects in the torus-like shape of the isosurfaces defined in its domain. The water molecule, on the contrary, breaks the linear symmetry, and thus does not permit for continuous attractors. In this case one can see, in addition to two isosurfaces in the CH bond basins, one “bean”-shaped isosurface, that contains two point attractors on each side of the Oxygen atom. Each irreducible domain, corresponding to each of these two attractors, contains two electrons.

Figs. 4 and 5 present another case: the formalimine molecule (also referred to as the smallest imine, or as the smallest unprotonated Schiff base). This molecules presents a double bond between Carbon and Nitrogen, and a lone pair attached to the Nitrogen atom. The upper figures of Fig. 4 depict the electronic density: an isosurface on the

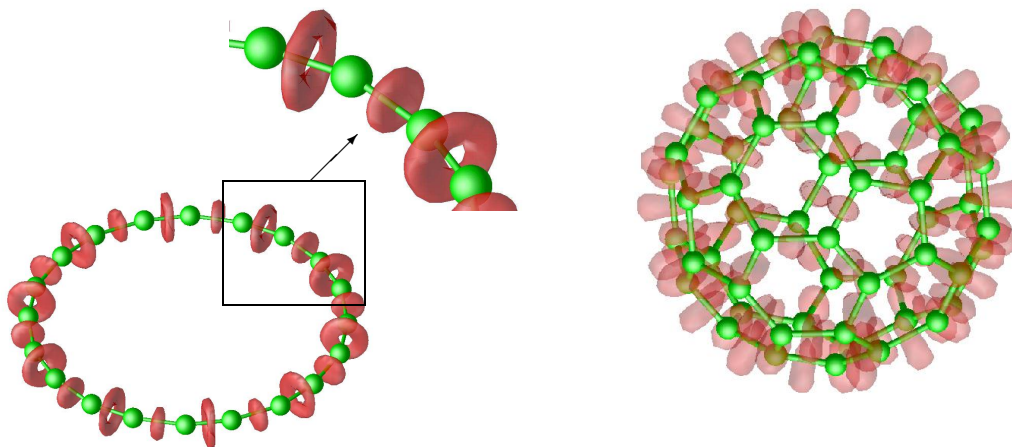


FIG. 2: ELF isosurfaces ( $\eta = 0.85$ ) for the ring isomer of  $C_{20}$  (left), and for the  $C_{60}$  fullerene.

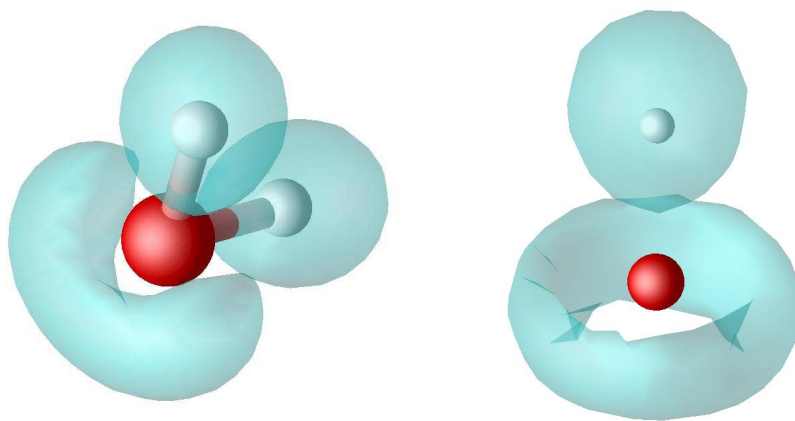


FIG. 3: ELF isosurfaces ( $\eta = 0.85$ ) of the water molecule (left), and of the hydroxide ion (right), showing the very different shape of the lone pair basin with four electrons (two point attractors, as it is the case for water), and with six electrons (ring-shaped attractor, as it is the case for the hydroxide ion).

left, and a logarithmic color map on the plane of the molecule on the right. Below, the figures depict the ELF in the same way – although the scale of the colormap in this case is not logarithmic. Both the bond (and its type) and the lone pair are clearly visible in the ELF, whereas the density presents much less structure.

Fig. 5 displays the same formaldehyde molecule; however, it shows the gradient lines of the ELF, which converge in the attractors. This alternative pictorial representation is also helpful to identify the positions of the attractors.

### C. Fast processes

The following time-dependent calculations of the ELF have been done by making use of TDDFT to describe the many-electron system. On top of this, the ions are also allowed to move. These are treated classically as point particles (the next subsection describes a model in which this restriction is lifted). The forces that define the ionic movement are calculated through Ehrenfest's theorem. It amounts to the simultaneous and coupled evolution of both a classical and a quantum system. The resulting Molecular Dynamics is non-adiabatic, since the electrons may occupy any excited state, and change these occupations.

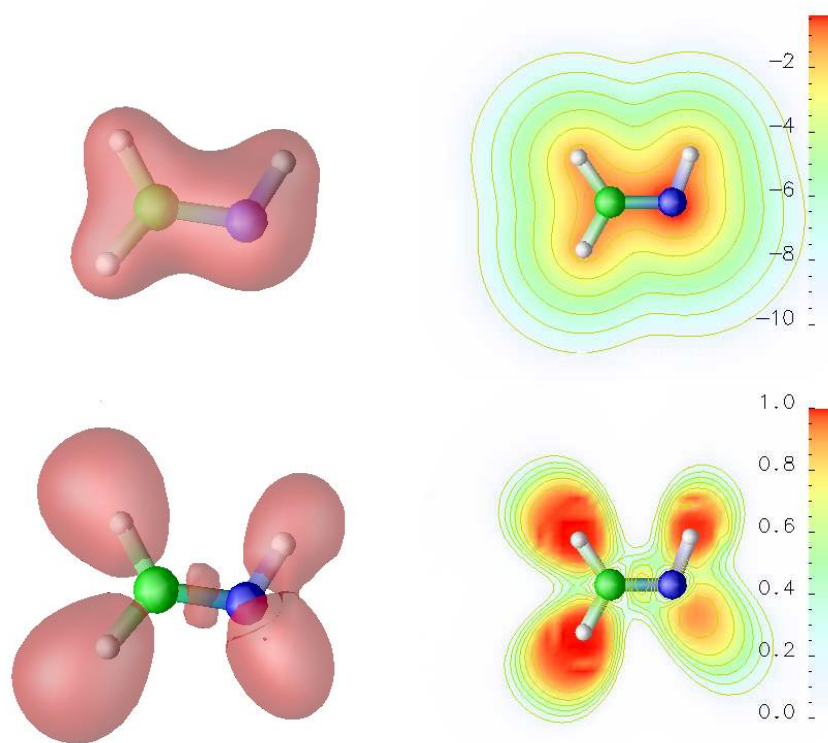


FIG. 4: Electronic density (top) and ELF (bottom, see text for its definition) of the ground state of the formaldehyde molecule. Left figures show one three dimensional isosurface, whereas the right figures show a colour-mapped two dimensional plane. Note that the scale in the case of the density is logarithmic; the values in the legend reflect the exponent.

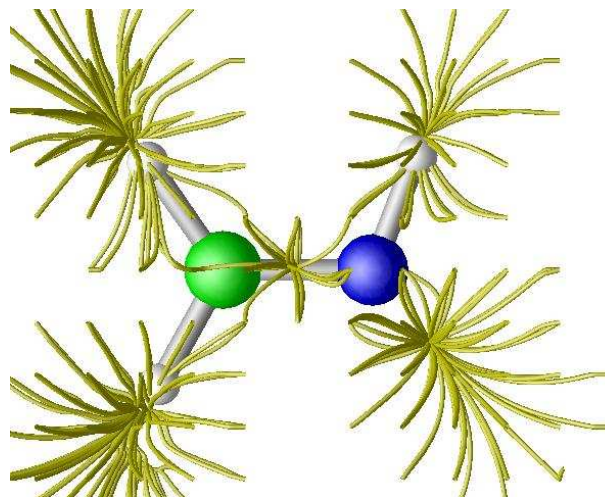


FIG. 5: Streamlines running through the gradient field of the ELF of formaldehyde, and meeting at the basin attractors – the ELF local maxima.

1. *The  $\text{H}^+ + \text{OH}^- \rightarrow \text{H}_2\text{O}$  reaction.*

In the following, the TDELf is used to monitor, “in real time”, the chemical behavior of the electrons involved in a chemical reaction. In this case, a specially simple one: the formation of a water molecule after the collision of a proton and a  $\text{OH}^-$  group.

One should recall, first of all, the topological differences between the lone-pair basin in the water molecule, containing two pairs, and the ring-shaped basin of the hydroxide ion (see Fig. 3). The chemical reaction that produces water should involve the transformation of this lone-pair basin. The collision of the two reactants produces different results depending on the original velocities and orientations; Two typical outcomes are presented here: a successful event (meaning formation of water), and an unsuccessful collision, leading to three isolated nuclei.

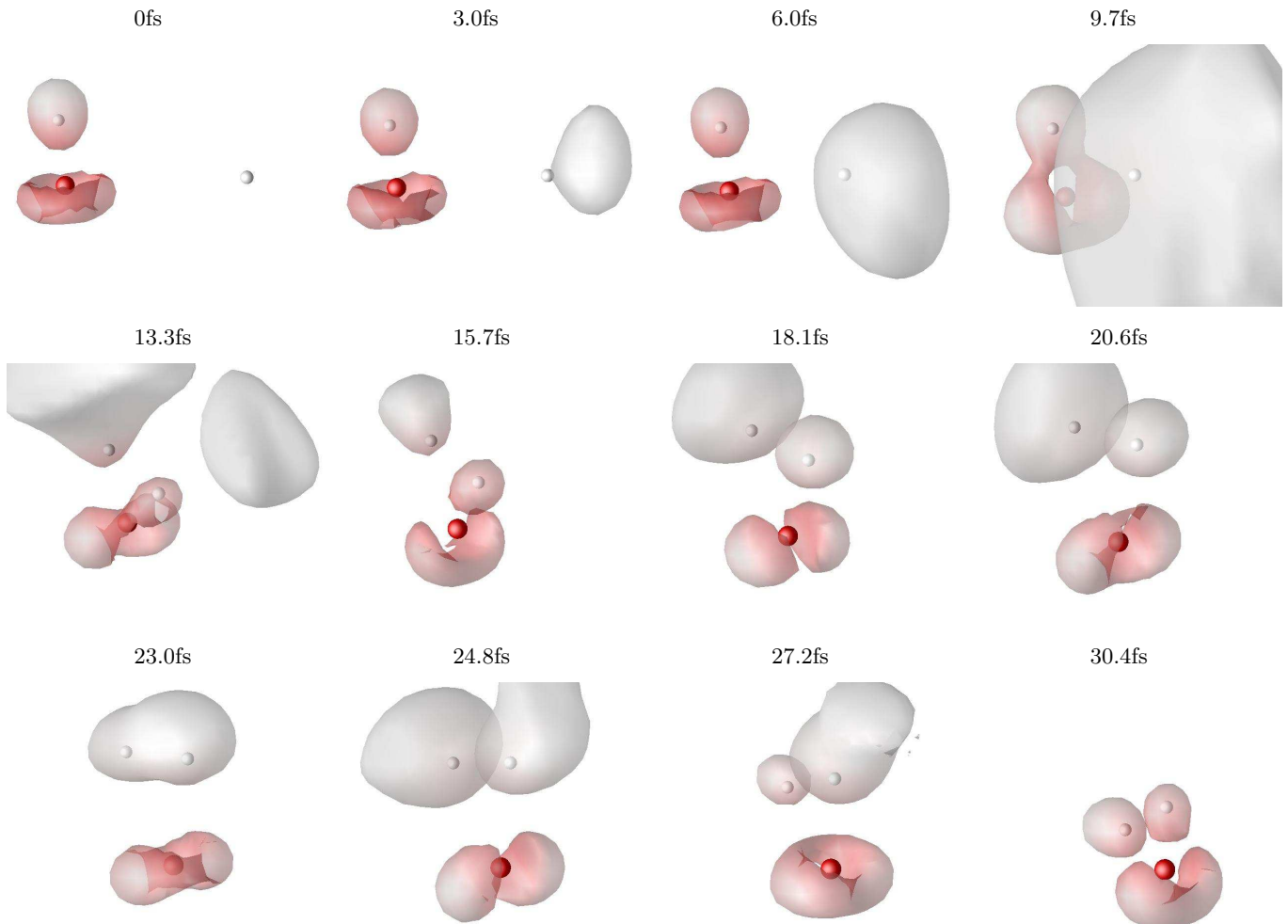


FIG. 6: Snapshots taken during the formation of a water molecule due to the collision of a proton and a  $\text{OH}^-$  group. Isosurfaces for the ELF at a value of  $\eta = 0.8$  are shown in red. This red color, however, is graduated depending on the local value of the electronic density: more intense red means higher density. The white areas, thus, correspond to regions of high electronic localization but low density. The Oxygen core is colored in red, whereas the protons are colored in white.

Fig. 6 shows the first of these two cases. At time zero, one can identify the characteristic ELF of the ground-state hydroxide ion. Note that this figure depicts isosurfaces of the ELF at a value of  $\eta = 0.8$ , and these isosurfaces are color-coded: an intense red means a region of high electronic density, whereas the whitish areas correspond to regions of almost negligible density. This is done in order to make apparent one of the less intuitive features of the ELF: it may have large values in regions of low electronic density.

The proton and the hydroxide group initially approach each other with a velocity of  $10^{-2}$  a.u., or  $0.21 \text{ \AA}/\text{fs}$ . The proton is directed to the middle point of the ion. As the proton approaches the hydroxide group in the first snapshots, an accumulation of ELF becomes apparent near it. This corresponds to a small transfer of electronic density – even if

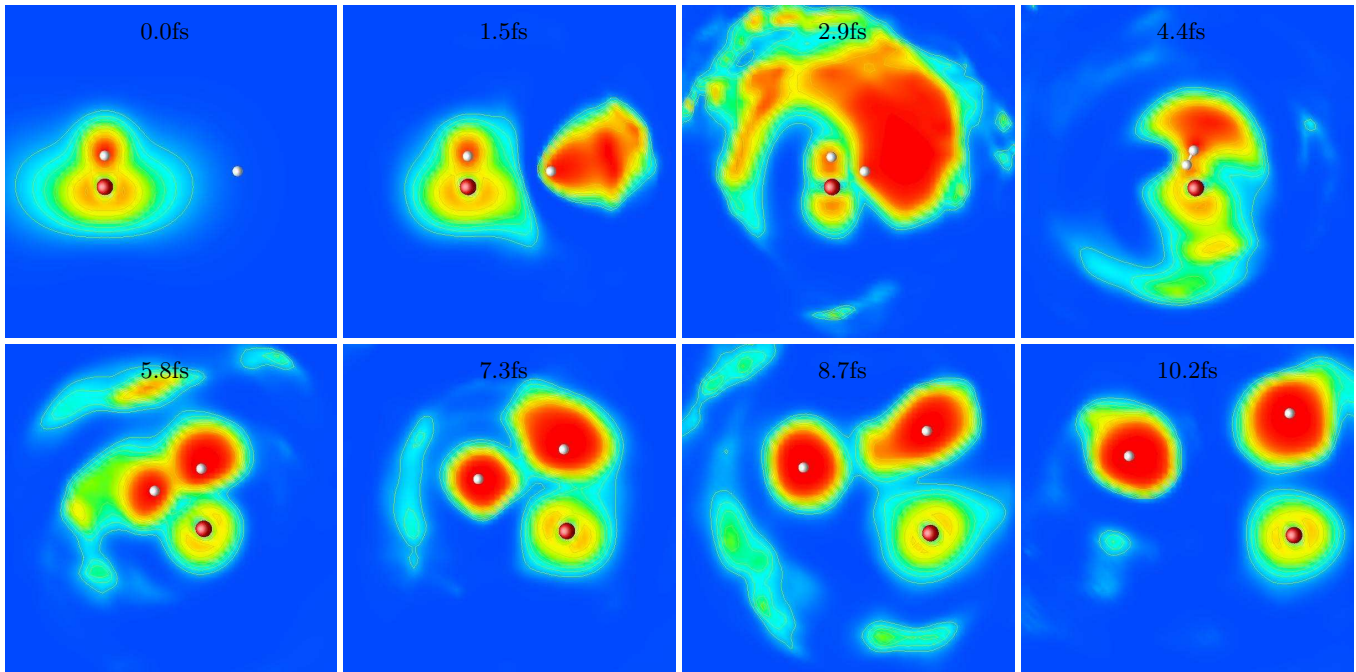


FIG. 7: Snapshots taken during the collision of a hydroxide ion with a proton, leading to the dissociation of the hydroxide group.

this density will be strongly localized and very large in size (see that snapshot taken at 9.7 fs), the amount of charge transfer is minute. This fact may be learnt from the lack of red color in this isosurface.

In the snapshots of the second row, the proton collides with the hydroxide group, and as a result the two protons jump away off the Oxygen atom. Each proton has now its associated ELF basin, whereas the lone pairs basin associated to Oxygen is already distorted. The last snapshots in the third row show the return of the protons to the influence of the Oxygen core, which demonstrates that water has been formed. The very last snapshot, some 30 fs after the process was initiated, clearly depicts the lone-pairs basin with the typical “bean” shape corresponding to two electron pairs. Note, however, that both nuclear and electronic degrees of freedom are in highly excited state, and thus the final picture is not a steady structure.

Fig. 7 shows another possibility, which occurs for higher proton velocities. In this case, the simulation is illustrated with a different representation procedure: a color map on the plane in which the three atoms move. The initial geometry is similar, but in this case the relative velocity is  $5 \cdot 10^{-2}$  a.u., or  $1.1 \text{ \AA/fs}$ . Once again, the second snapshot shows how a cloud of localized electrons develops around the proton as it approaches the anion. It becomes specially large after 2.9 fs; note however that it does not mean a large electronic transfer; to learn about that one needs to look at the density. In the fourth snapshot, the incoming proton cleanly passes through the bond. The original shape of the ELF is completely distorted; however the speed of the process did not allow yet for fast movements of the nuclei – except the straight line movement due to their original velocities.

In the second row one may see the proton scatter away from the anion; it does so at an angle from its initial trajectory. The bond of the anion is broken; as a consequence the two nuclei separate from each other. Each of the three nuclei carries away an electronic cloud: a spherical crown in the case of the Oxygen atom (corresponding to the typical two dimensional spherical attractor of an isolated many electron atom), and spatially large accumulations of localized electrons for the protons (note, once again, that this does not imply a large number of electrons. In order to learn about the electronic charge carried away by each of the ions, it is necessary to integrate the density in each of the localization domains).

## 2. Proton capture by a lone pair

The next case focuses in the formaldehyde molecule, Fig. 5. It presents one lone pair, which chemically may behave as a possible anchorage for a radical. For example, it may attract a “traveling” proton in an acid environment. This is demonstrated in the simulation depicted in Fig. 8.

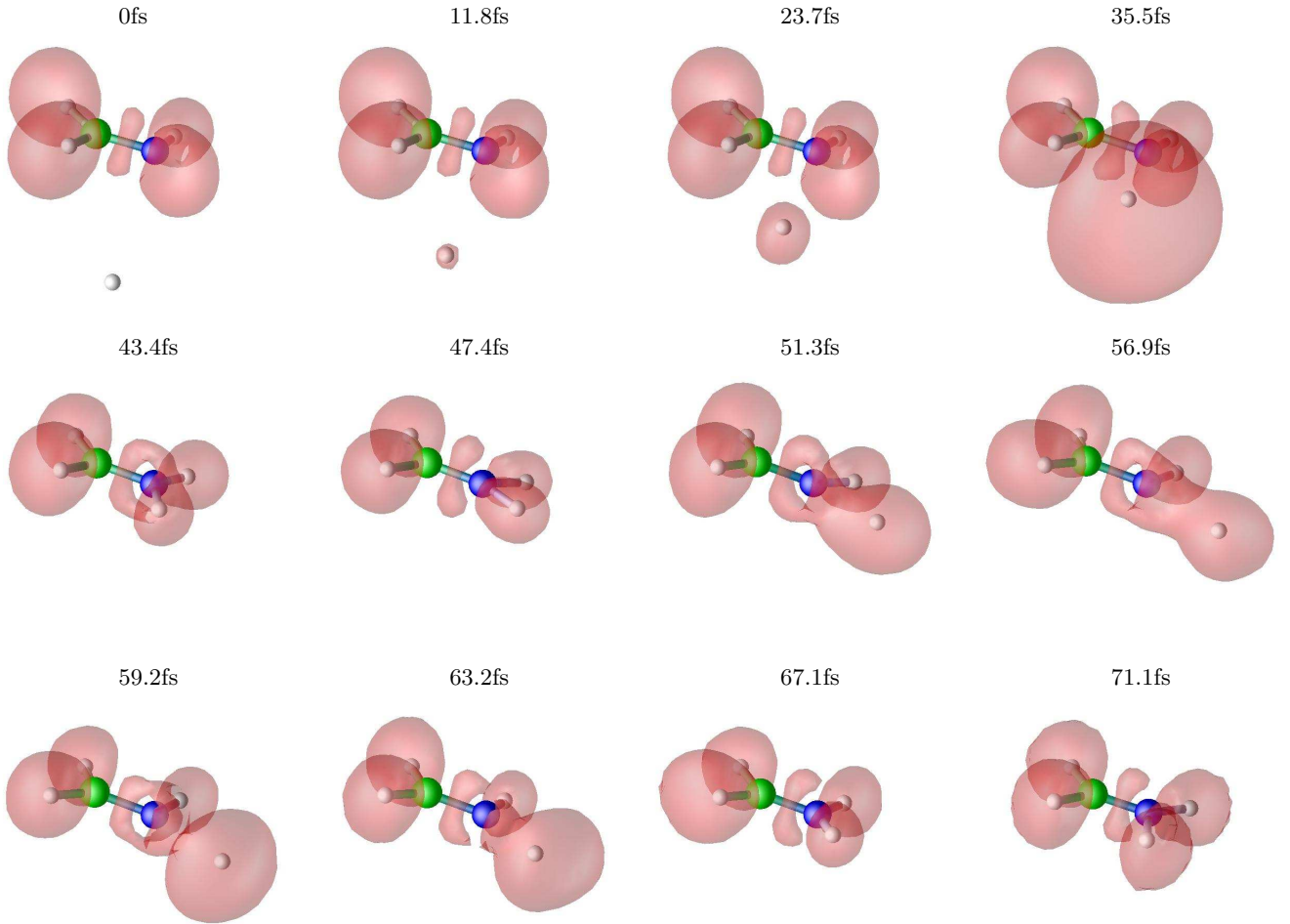


FIG. 8: Snapshots taken during the capture of a proton by a formalimine molecule. Isosurfaces for the ELF at a value of  $\eta = 0.8$  are shown in red. The Carbon and Nitrogen cores are colored in green and blue respectively, whereas the protons are colored in white.

In the first snapshot, the formalimine molecule is in its ground state, both its electronic and nuclear degrees of freedom. The topology of the ELF for this particular case was discussed in the previous subsection. A proton travels with a velocity of  $5.2 \cdot 10^{-3}$  atomic units (corresponding to an energy of 0.673 eV), in the plane of the molecule, and initially aiming to the center of the CN double bond. The lone pair, however, attracts the proton to its basin. As a result, the proton drifts to the right, in the direction of the Nitrogen atom, accelerating its movement. The molecule itself also rotates as the Nitrogen atom attempts to approach the incoming proton. This enters the non-bonding basin, and transforms it into a bonding NH lobe. The ensuing collision results in the proton quickly accelerating out of the molecule; however, the bond has been established, and soon it is driven back. The result is a highly excited molecule: the nuclei will vibrate, whereas the electronic state will also be a mixture of the ground state and higher lying states. Of course, eventually it could relax upon photon emission; this is however not included in the model.

### 3. Bond-breaking by an intense, ultrafast laser pulse

The next example shows the excitation of the ethyne molecule by means of a strong laser. The aim is especially the triple bond. The laser is polarized along the molecular axis; it has a frequency of 17.15 eV ( $\lambda = 72.3$  nm) and a maximal intensity of  $I_0 = 1.19 \times 10^{14}$  W/cm<sup>2</sup>. Fig. 9 depicts snapshots of the ELF of acetylene in form of slabs through a plane of the molecule. At the beginning (a) the system is in the ground state and the ELF visualizes these features: The torus between the Carbon atoms, which is typical for triple bonds, and the blobs around the Hydrogen

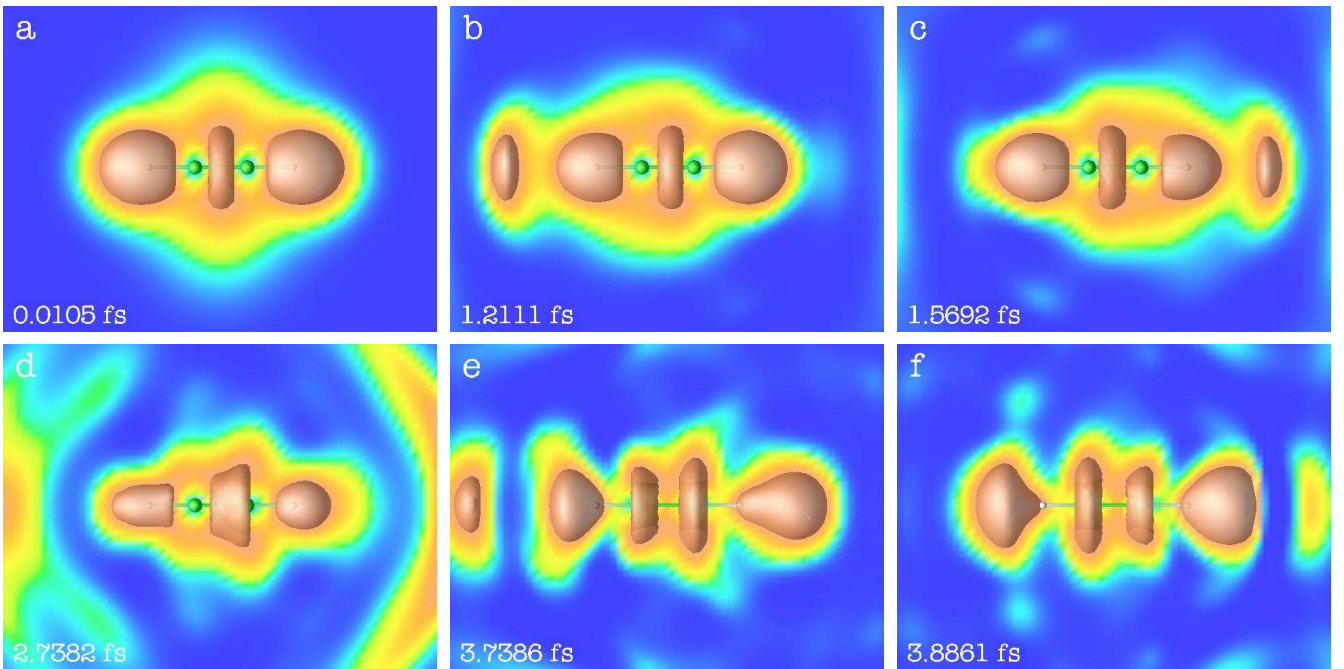


FIG. 9: Snapshots of the time-dependent ELF for the excitation of ethyne (acetylene) by a 17.15 eV ( $\lambda=72.3$  nm) laser pulse. The pulse had a total length of 7 fs, a maximal intensity of  $1.2 \times 10^{14}$  W/cm<sup>2</sup>, and was polarized along the molecular axis. Ionization and the transition from the bonding  $\pi$  to the anti-bonding  $\pi^*$  are clearly visible.

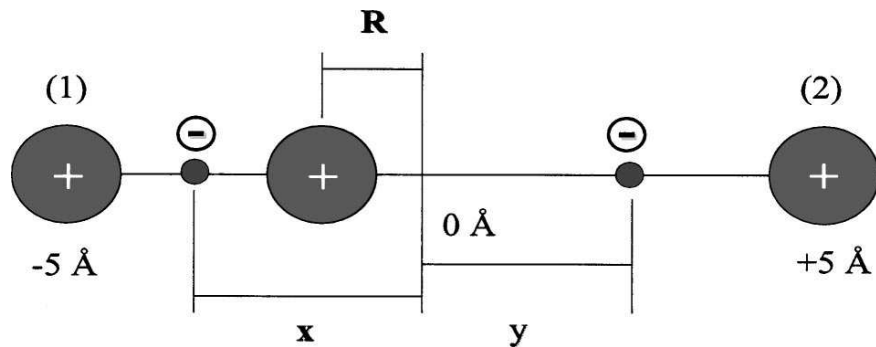


FIG. 10: Configuration of the model system: An ion (coordinate  $R$ ) and two electrons (at  $x$  and  $y$ ) are allowed to move between two fixed ions (1) and (2), fixed at a distance of 10 Å.

atoms. As the intensity of the laser increases, the system starts to oscillate and then ionizes (Fig. 9b,c). Note that the ionized charge leaves the system in fairly localized packets (the blob on the left in b, and on the right in c). The central torus then starts to widen (Fig. 9d) until it breaks into two tori centered around the two Carbon atoms (Fig. 9e,f). This can be interpreted as a transition from the  $\pi$  bonding to the  $\pi^*$  non-bonding state. The system then remains in this excited state, and eventually dissociates, after the laser has been switched off. In the process, the molecule absorbs about 60 eV of energy, and loses 1.8 electrons through ionization.

#### D. TDELf for coupled nuclear-electronic motion

The examples presented in the previous subsection neglected the quantum nature of the atomic nuclei. Erdmann, Gross and Engel<sup>32</sup> have presented one application of the TDELf for a model system in which one nucleus is treated quantum mechanically, and the full Schrödinger equation is computed exactly. This model is specially suited to study, from a fundamental point of view, the effects of non-adiabaticity. It is instructive to see how the ELF may help for this purpose.

The model is depicted in Fig. 10: two electrons and a nucleus that move in a single dimension between two fixed ions. Its Hamiltonian is:

$$H(x, y, R) = T(x) + T(y) + T(R) + V(x, y, R), \quad (24)$$

where  $T(x)$ ,  $T(y)$  and  $T(R)$  are the kinetic energy operator of the two electrons and of the moving ion, respectively. The potential is:

$$\begin{aligned} V(x, y, R) = & \frac{Z_1 Z}{|R_1 - R|} + \frac{Z_2 Z}{|R_2 - R|} + \frac{\text{erf}(|x - y|)}{R_e |x - y|} \\ & - \frac{Z_1 \text{erf}(|R_1 - x|)}{R_f |R_1 - x|} - \frac{Z_2 \text{erf}(|R_2 - x|)}{R_f |R_2 - x|} - \frac{Z \text{erf}(|R - x|)}{R_c |R - x|} \\ & - \frac{Z_1 \text{erf}(|R_1 - y|)}{R_f |R_1 - y|} - \frac{Z_2 \text{erf}(|R_2 - y|)}{R_f |R_2 - y|} - \frac{Z \text{erf}(|R - y|)}{R_c |R - y|}. \end{aligned} \quad (25)$$

Note that the interactions are screened; The values of the screening are modulated by the parameters  $R_f$  (for the interaction electron – fixed ions),  $R_c$  (for the interaction electron – moving ion), and  $R_e$  (for the electron – electron interaction). By tuning these parameters, the non-adiabatic couplings may be reduced or enhanced<sup>33–37</sup>.

The degree of diabaticity is qualitatively pictured in the adiabatic potential energy surfaces (PES) – which show the eigenvalues, parameterized with the nuclear coordinate  $R$ , of the electronic equation:

$$\{T(x) + T(y) + V(x, y, R)\} \phi_n^{\sigma\tau}(x, y; R) = V_n^{\sigma\tau}(R) \phi_n^{\sigma\tau}(x, y; R), \quad (26)$$

so that  $\phi_n^{\sigma\tau}(x, y; R)$  are the electronic eigenfunctions in state  $n$ . Two different initial configurations are possible: the two electrons are in the same spin state – corresponding to spatial functions of gerade symmetry –, or in opposite spins – corresponding to ungerade spatial functions. (Note that since the full Hamiltonian does not contain the spin, the system will remain in the same spin configuration during any evolutions). The adiabatic PES are depicted in Fig. 11 for the anti-parallel spin (top) and parallel spin (bottom) cases, and for the ground state, and the first three excited states.

In the anti-parallel case, the ground state and the first excited state show an avoided crossing, so we should expect clear non-adiabatic behavior in that region. In the parallel spin case, however, the ground state and the first excited state are well separated from each other and from the higher states, whereas the second and third excited states again show avoided crossings.

The localization functions for this particular model have to be defined. The full time-dependent density matrix is given by:

$$D_{\sigma\tau}(x, y, R; t) = |\Psi(x\sigma, y\tau, R; t)|^2, \quad (27)$$

where  $\Psi$  is the full wave function. Integrating out the nuclear degree of freedom, one obtains the density matrix for the two electrons:

$$D_{\sigma\tau}(x, y; t) = \int d^3 R D_{\sigma\tau}(x, y, R; t), \quad (28)$$

and one may then define the conditional pair probability function:

$$P_{\sigma\tau}(x, y; t) = \frac{D_{\sigma\tau}(x, y; t)}{\rho_\sigma(x; t)}, \quad (29)$$

where  $\rho_\sigma$  is the electronic one-particle spin-density. Two cases have to be distinguished:

1. Anti-parallel spins:  $P_{\alpha\beta}(x, x; t)$  is the conditional probability to find one electron at time  $t$  at point  $x$ , if we know with certainty that other electron with opposite spin is in the same place. This is an indirect measure of localization. One may define, in analogy to the usual ELF, a time-dependent *anti-parallel spin* electron localization function (TDALF),  $\eta^{\text{ap}}$ , as:

$$\eta^{\text{ap}}(x; t) = \frac{1}{1 + |P_{\alpha\beta}(x, x; t)/F_\alpha(x; t)|^2}. \quad (30)$$

$F_\alpha(x; t) = (4/3)\pi^2 \rho_\alpha^3(x; t)$  is the Thomas-Fermi kinetic energy density for anti-parallel spins and 1D systems.

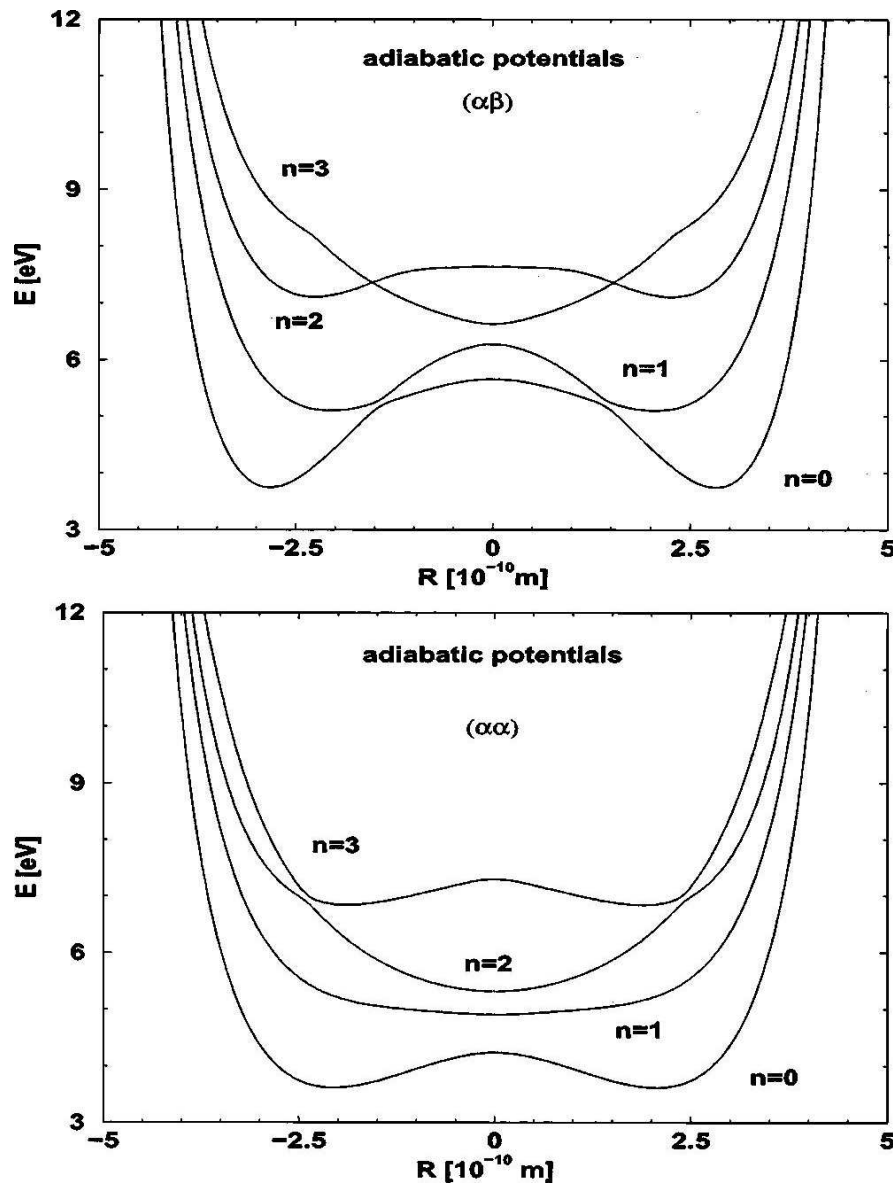


FIG. 11: Adiabatic potentials for the anti-parallel (top panel) and parallel spin case (bottom panel). Different parameters were used in the parametrization of the interaction energy:  $R_c = R_f = 1.5 \text{ \AA}$ ;  $R_e = 2.5 \text{ \AA}$  (left panel), and  $R_c = R_f = R_e = 1.5 \text{ \AA}$  (right panel).

2. Parallel spins: This would correspond to the usual ELF, presented previously. However, the one-dimensionality of the model changes the derivation since the spherical average is not necessary. Defining  $s = x - y$ , one may expand  $P_{\alpha\alpha}(x, s; t)$  in a Taylor series up to second order around  $s = 0$ :

$$P_{\alpha\alpha}(x, s; t) = \frac{1}{2} \frac{\partial^2 P_{\alpha\alpha}}{\partial s^2}(x, 0; t) s^2 + \mathcal{O}(s^3). \quad (31)$$

The constant term is null due to Pauli's principle, whereas the linear term also vanishes since, according to Kato's cusp theorem<sup>38</sup>, the wave function is proportional to  $s$ . The  $s^2$  coefficient,  $a_{\alpha\alpha}(x; t)$ , is now used to define the TDELFF with the usual re-normalization precautions:

$$\eta(x; t) = \frac{1}{1 + |a_{\alpha\alpha}(x; t)/F_{\alpha}(x, t)|^2}. \quad (32)$$

In this case,  $F_{\alpha}(x) = (16/3)\pi^2\rho_{\alpha}^3(x)$ .

The nuclear movement is investigated through the time-dependent nuclear density:

$$\Gamma_{\sigma\tau}(R; t) = \int d^3x \int d^3y D_{\sigma\tau}(x, y, R; t). \quad (33)$$

The time-evolution of the system is then initiated from an initial state with the form:

$$\Psi(x\sigma, y\tau, R; t = 0) = e^{-\gamma(R-R_0)^2} \phi_n^{\sigma\tau}(x, y; R), \quad (34)$$

that is, from the first electronic excited state, and from a Gaussian nuclear distribution around some initial point – in this case,  $R_0 = -3.5 \text{ \AA}$ .

Once again, two possible spin configurations for the initial state have to be distinguished:

1. Anti-parallel spins.

This case is shown in Fig. 12, left side. The top graph represents the *nuclear* time-dependent density. This density, initially localized around  $-3.5 \text{ \AA}$ , travels towards its turning point, while it strongly disperses. Soon, as a consequence of the strong non-adiabatic coupling, the nuclear wave packet becomes extremely broad and a defined structure can no longer be seen.

The electron density (middle panel) seems to be unaware of the nuclear motion. This does not mean that electrons are static; its behavior may be best analyzed by looking at the TDALF (lower panel). We have two localization domains, which correspond also with the initial areas of high density. It may be seen how, as the nucleus transverses this area, the localization amplitude diminishes, and almost vanishes for those two areas. This illustrates how the strong non-adiabatic coupling is effective in decreasing localization.

2. Parallel spins.

This case is shown in Fig. 12, right side. Also, the nuclear time-dependent density is on the top and the time-dependent electron density is in the middle, although in this case it is the usual TDELf (parallel-spins) which is shown in the bottom panel.

This case has been tailored to avoid the presence of non-adiabatic effects (the first excited state is well separated from the others). As a result, with the chosen initial conditions, the motion takes place exclusively in a single electronic state. The nuclear wave packet is initially localized in the left half of the potential well, and starts moving to the right side where it is repelled by the right side fixed ion at about 40 fs. The wave packet then shows an oscillatory structure, and broadens due to the anharmonicity of the potential.

The electronic density reflects a charge transfer from the left fixed ion to the right one, with the moving ion acting as an “electron carrier”. Initially, there are two maxima in the vicinity of the left fixed ion and on the moving one. After the nucleus crosses the origin, the initial density drops to zero and the new two maxima are on top of the moving ion and on the right side. If the nucleus were not affected by dispersion, the process would reverse with each half-cycle of the nuclear vibration.

The behavior of the TDELf is now very different with respect to the TDALF in the anti-parallel spin case. The localization remains high at all times, and the transfer of electrons from left to right is clear: Initially there are two localization domains; one around the fixed ion, and another near the origin. As the nuclear movement starts, the first domain vanishes, and a third domain appears near the right fixed ion. After the vibrational period of the nucleus is finished, this third domain disappears, and the initial ELF is however restored. The vanishing of the first domain and the appearance of a third domain indicates that one electron must have been removed from the left fixed nucleus and dragged to the right.

In conclusion, the handful of examples presented in this section illustrate the amount of information that can be gained from the time-dependent ELF in theoretical studies of ultrafast phenomena. One can learn about the time scales of the processes, and/or about how the various sub-events that make up a complex reaction are ordered in time: which bonds break first, which second, how the new links are created, etc. One can observe and interpret intermediate electronic structure that may be short lived but relevant for the overall outcome. This information starts to become available to experimentalists, as the time resolution of the sub-femtosecond laser sources increases.

---

<sup>1</sup> G.N. Lewis, Journal of the American Chemical Society **38**(4), 762 (1916)

<sup>2</sup> T. Brabec, F. Krausz, Rev. Mod. Phys. **72**(2), 545 (2000)

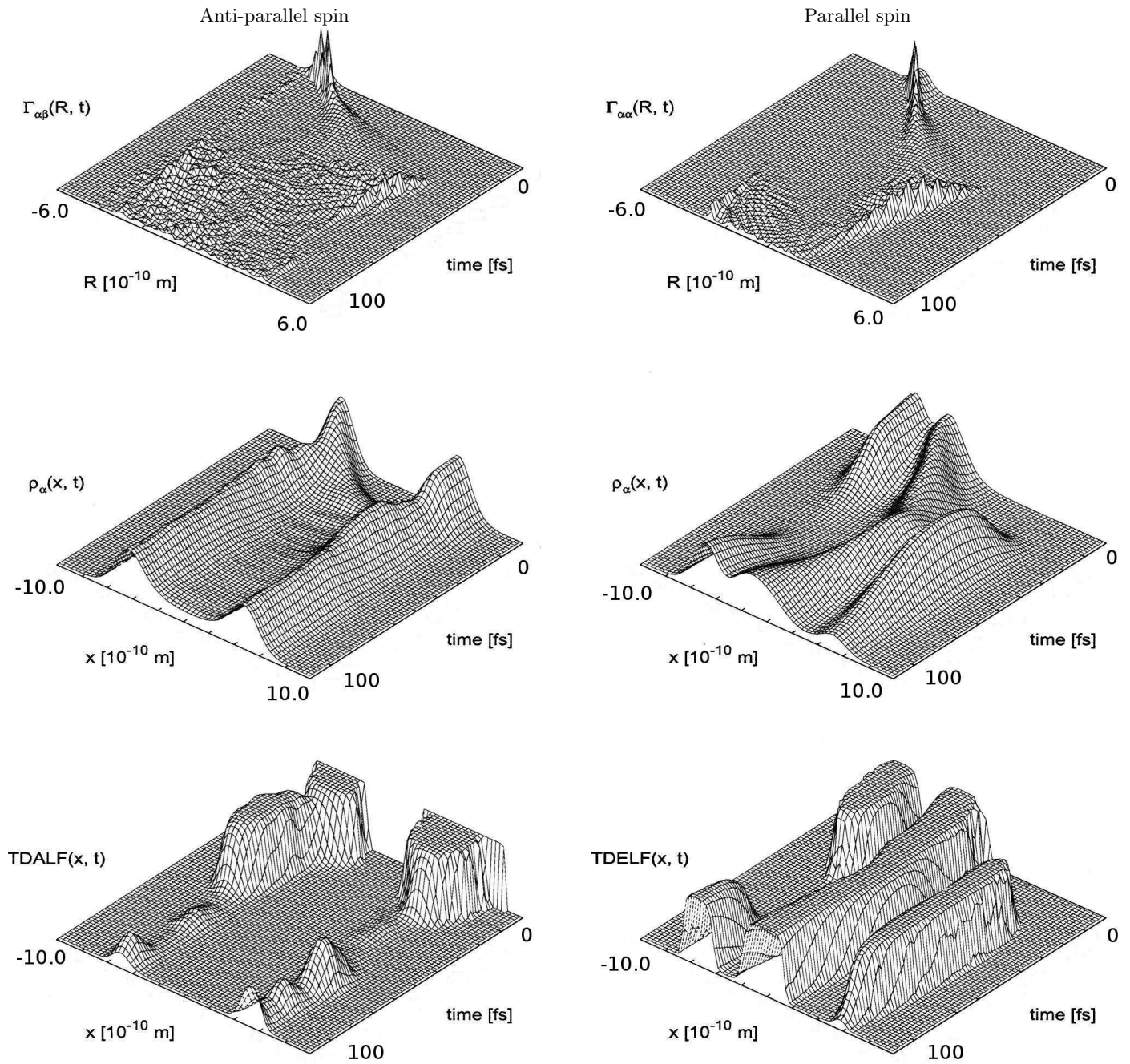


FIG. 12: Quantum dynamics of the model system presented in Sect. D, for the anti-parallel spin (left) and the parallel spin cases (right). The upper panel shows the nuclear density. The time-dependent electron density and TDELf are shown in the middle and lower panels, respectively.

- <sup>3</sup> P.M. Paul, E.S. Toma, P. Breger, G. Mullot, F. Audebert, P. Balcou, H.G. Muller, P. Agostini, *Science* **292**(5522), 1689 (2001)
- <sup>4</sup> C. Edmiston, K. Ruedenberg, *Rev. Mod. Phys.* **35**(3), 457 (1963)
- <sup>5</sup> W. Kohn, L.J. Sham, *Physical Review* **140**(4A), A1133 (1965)
- <sup>6</sup> C. Fiolhais, F. Nogueira, M.A.L. Marques (eds.), *A Primer in Density Functional Theory, Lecture Notes in Physics*, vol. 620 (Springer, Berlin, 2003)
- <sup>7</sup> R.M. Dreizler, E.K.U. Gross, *Density Functional Theory* (Springer, Berlin, 1990)
- <sup>8</sup> R.G. Parr, W. Yang, *Density-Functional Theory of Atoms and Molecules* (Oxford University Press, New York, 1989)
- <sup>9</sup> P. Hohenberg, W. Kohn, *Physical Review B* **136**(3B), B864 (1964)
- <sup>10</sup> R.F.W. Bader, S. Johnson, T.H. Tang, P.L.A. Popelier, *Journal of Physical Chemistry* **100**(38), 15398 (1996)
- <sup>11</sup> A.D. Becke, K.E. Edgecombe, *J. Chem. Phys.* **92**(9), 5397 (1990)
- <sup>12</sup> T. Burnus, M.A.L. Marques, E.K.U. Gross, *Phys. Rev. A* **71**(1), 010501 (2005)
- <sup>13</sup> Y. Tal, R.F.W. Bader, *International Journal of Quantum Chemistry* **12**, 153 (1978)
- <sup>14</sup> J.F. Dobson, *J. Chem. Phys.* **98**(11), 8870 (1993)
- <sup>15</sup> P.O. Löwdin, *Physical Review* **97**(6), 1474 (1955)
- <sup>16</sup> R. McWeeny, *Rev. Mod. Phys.* **32**(2), 335 (1960)
- <sup>17</sup> A.D. Becke, *International Journal of Quantum Chemistry* **23**(6), 1915 (1983)
- <sup>18</sup> T. Burnus, Time-dependent electron localization function. Diplomathesis, Freie Universität Berlin (2004)
- <sup>19</sup> E. Runge, E.K.U. Gross, *Phys. Rev. Lett.* **52**(12), 997 (1984)
- <sup>20</sup> M.A.L. Marques, F. Nogueira, C. Ullrich, K. Burke, A. Rubio, E.K.U. Gross, *TDDFT. Lecture notes* (Springer, Berlin, to be published in 2006)
- <sup>21</sup> M.A.L. Marques, E.K.U. Gross, *Annual Review of Physical Chemistry* **55**, 427 (2004)
- <sup>22</sup> R. van Leeuwen, *Int. J. Mod. Phys. B* **15**(14), 1969 (2001)
- <sup>23</sup> E. Gross, J. Dobson, M. Petersilka, in *Topics in Current Chemistry*, vol. 181, ed. by R.F. Nalewajski (Springer, Berlin, 1996), pp. 81–172
- <sup>24</sup> E.K.U. Gross, W. Kohn, *Adv. Quantum Chem.* **21**, 255 (1990)
- <sup>25</sup> A. Savin, R. Nesper, S. Wengert, T.F. Fässler, *Angewandte Chemie-International Edition in English* **36**(17), 1809 (1997)
- <sup>26</sup> M. Kohout, A. Savin, *Journal of Computational Chemistry* **18**(12), 1431 (1997)
- <sup>27</sup> J.B. Krieger, Y. Li, G.J. Iafrate, *Phys. Rev. A* **46**(9), 5453 (1992)
- <sup>28</sup> A. Castro, H. Appel, M. Oliveira, C.A. Rozzi, X. Andrade, F. Lorenzen, M.A.L. Marques, E.K.U. Gross, A. Rubio, *physica status solidi (b)* p. in press (2006)
- <sup>29</sup> M.A.L. Marques, A. Castro, G.F. Bertsch, A. Rubio, *Comput. Phys. Commun.* **151**(1), 60 (2003)
- <sup>30</sup> B. Silvi, A. Savin, *Nature* **371**(6499), 683 (1994)
- <sup>31</sup> D.B. Chesnut, *J. Phys. Chem. A* **104**(49), 11644 (2000)
- <sup>32</sup> M. Erdmann, E.K.U. Gross, V. Engel, *J. Chem. Phys.* **121**(19), 9666 (2004)
- <sup>33</sup> S. Shin, H. Metiu, *J. Chem. Phys.* **102**(23), 9285 (1995)
- <sup>34</sup> S. Shin, H. Metiu, *Journal of Physical Chemistry* **100**(19), 7867 (1996)
- <sup>35</sup> M. Erdmann, P. Marquetand, V. Engel, *J. Chem. Phys.* **119**(2), 672 (2003)
- <sup>36</sup> M. Erdmann, V. Engel, *J. Chem. Phys.* **120**(1), 158 (2004)
- <sup>37</sup> M. Erdmann, S. Baumann, S. Gräfe, V. Engel, *Eur. Phys. J. D* **30**(3), 327 (2004)
- <sup>38</sup> T. Kato, *Commun. Pure Appl. Math.* **10**(2), 151 (1957)
- <sup>39</sup> It may be argued that the ELF that we depict, is, in fact, a pseudo-ELF. The effect of removing the core electrons in the ELF is the removal of localized electrons in the vicinity of the nuclei. This is irrelevant if one is interested in learning about the chemical properties of the systems.